Multi-crease Self-folding by Global Heating

Shuhei Miyashita*,**
Massachusetts Institute of Technology

Cagdas D. Onal†
Worcester Polytechnic Institute

Daniela Rus**
Massachusetts Institute of Technology

Abstract This study demonstrates a new approach to autonomous folding for the body of a 3D robot from a 2D sheet, using heat. We approach this challenge by folding a 0.27-mm sheetlike material into a structure. We utilize the thermal deformation of a contractive sheet sandwiched by rigid structural layers. During this baking process, the heat applied on the entire sheet induces contraction of the contracting layer and thus forms an instructed bend in the sheet. To attain the targeted folding angles, the V-fold spans method is used. The targeted angle θ_{out} can be kinematically encoded into crease geometry. The realization of this angle in the folded structure can be approximately controlled by a contraction angle θ_{in}. The process is non-reversible, is reliable, and is relatively fast. Our method can be applied simultaneously to all the folds in multi-crease origami structures. We demonstrate the use of this method to create a lightweight mobile robot.

Keywords
Heat-based multi-crease self-folding, fold angle control, V-fold spans, morphogenetic fabrication, self-assembly

1 Introduction

The remarkable capability of bio-entities in developing a morphology is called morphogenesis. As robots enter our daily life and become more ubiquitous, demands for the instant fabrication of robots that can morph and are adaptive to various environments increase. This is a challenge that has been tackled in modular robotics, where a robot's body consisting of multiple modules reconfigures and adapts to environmental changes [4, 16, 25, 26, 35], or in a similar effort but attempting to handle highly stochastic situations in a bottom-up manner [5, 15, 19, 22], or a folding manner [2]. A unique approach focusing on extending a robot's physical capabilities is taken by [1], where the robot can print and use a three-dimensional tool.

Recently, the folding-based creation of robot bodies from sheetlike materials has shown notable accomplishments [8, 9, 34]. The methods employed in these works make frequent use of origami-inspired foldings to create lightweight mechanisms. Complex bodies can be folded from a laser-cut single sheet of paper [27, 28].

This article makes the following contributions:

1. a model, design, and method for designing flat origami structures that can self-fold in a controlled way, using global heating;

* Contact author.
** Computer Science and Artificial Intelligence Laboratory, Massachusetts Institute of Technology, 32 Vassar Street, 32-379, Cambridge, MA 02139, USA. E-mail: shuheim@csail.mit.edu (S.M.); rus@csail.mit.edu (D.R.)
† Worcester Polytechnic Institute, Department of Mechanical Engineering, Robotics Engineering Program, 100 Institute Rd., HL 105, Worcester, MA 01609, USA. E-mail: cdonal@wpi.edu

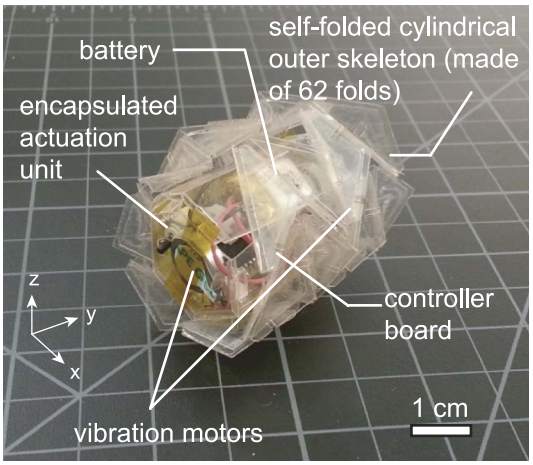

Figure 1. View of self-folded outer skeleton with a modularized actuation unit.

2. an instantiation of this approach to create a self-folding cylindrical-shaped robot and extensive experimental characterization.

The key insight is to use a flat sheet sandwiched by rigid structural layers. The structure of the hard layers determines the target angles that are achievable on each structural edge, which determine, in turn, the final geometry of the self-folded object. Next, we impose an origami crease pattern that was designed by hand and added to the robot's body using a laser cutter. Finally, we suspend the sheet in an oven. The self-folding process takes approximately 5 min at 65°C. The resulting shape is a textured cylinder. We add to this cylinder a printed circuit, supporting electronics, and vibration motors, and configure a locomotion robot. The robot can perform locomotion on a plane by altering the speeds of vibration motors (Figure 1). Creating robot bodies by self-folding is fast, easy, and inexpensive.

2 Self-folding Method

One of the requisite competencies for robots that morph from a sheet structure is self-folding capability. Various attempts at automating folding processes have been made [12], using shape memory alloys [7], a contraction sheet combined with Joule heating [3], light illumination for heat transfer [17, 31], pneumatic actuation coupled with an elastic body [18], or hydrogel expansion [6]. Nevertheless, few approaches have attempted to achieve the self-folding of large creased forms with a high degree of accuracy, or demonstrated a realistic fabrication time compared with the folding time.

The self-folding methodology described in this article, which is developed upon our previous work in [23, 24], consists of the following steps:

1. We model and derive a method for causing a bend on one edge of a flat body structure created by layering a contraction sheet and structural sheets and using global heating (Section 2.1).
2. We develop a method for designing 2D planar bridges and gaps in a layered sheet that enables multiple edges to be folded in parallel, using heat, to create different geometries.
3. We compute and control the angles to be folded using steps 1 and 2; the material and geometry of the creases determine the size of the angle that can be folded (Section 2.2).

4. We design a specific crease pattern to test the self-folding approach we advocate; this pattern can be folded reliably as a complete cylinder with patterned faces (Section 3.1).
5. We integrate electronics and actuators in the self-folded cylindrical body to create a lightweight mobile robot and demonstrate and characterize its locomotion.

2.1 Folding by Global Heating

The key insight is to transform the internal stress of a contraction sheet into a folding torque. Our goal is to globally heat the structure to induce simultaneous foldings. The idea is inspired by the natural and artificial chemical compounds' folding, as in [29]. We wish to apply the general concept to different scales. Figure 2 shows the designed mechanism for self-folding. We use a heat-sensitive contracting material (a polyvinyl chloride (PVC) shrink bag) for inducing shear force, which, in turn, creates the torque for bending a plane. (a) When a non-deformable structural layer is laminated to PVC from one side, the sheet structure forms a bend. (b) By sandwiching the PVC layer with structural layers with different gap widths, the gap width difference between the front and back of the sheet at the same position enables the control of the folding direction. Here, structural layers are acting to prevent most of the sheet from bending. (c) The approach is capable of folding mountain and valley folds simultaneously. Furthermore, the folding angles (θ_{h1} and θ_{h2} in Figure 2) can be approximately encoded with the gap widths [33]. In general, the wider W_h becomes, the steeper the folding angle becomes.

PVC has two ideal features: the capability of low-temperature contraction (below 100°C), and a robust physical structure with transparent visibility. PVC also has some disadvantages: The material naturally deforms, and it is weak and subject to tearing.

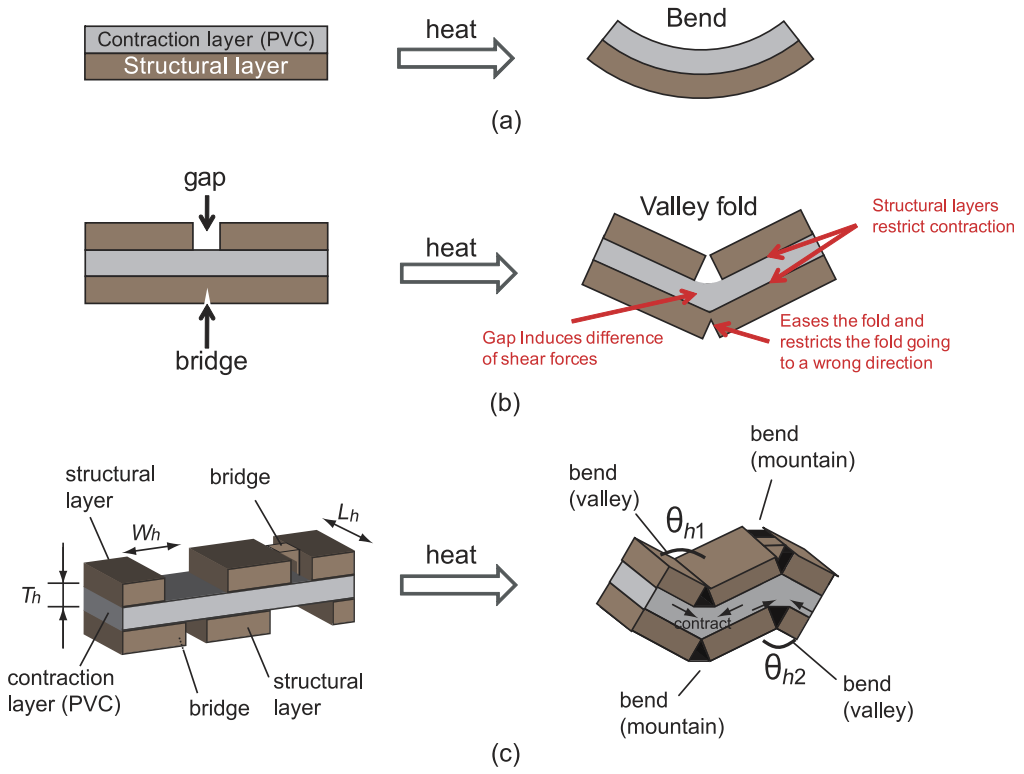

Figure 2. Proposed self-folding method using global heating. (a) Bending. (b) Folding to one side. (c) Folding to both sides.

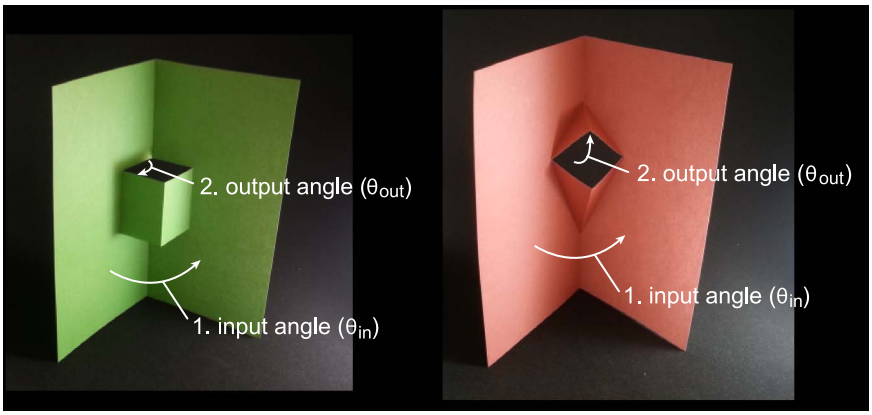

Figure 3. Two pop-up techniques: (a) parallel fold and (b) V-fold.

The required torque τ_h for generating the elastic deformation of a hinge is generally given by [13]

$$\tau_h = E_h \frac{W_h \cdot T_h^3}{12 L_h} \theta_h, \tag{1}$$

where E_h is the elastic modulus of the hinge; W_h, T_h, and L_h are the width, thickness, length of the hinge, respectively; and θ_h is the fold angle. For example, in Figure 2b,d, τ_1 at hinge 1 is 1.48×10^{-9} N m with values $E_h = 3$ MPa (approximate assumption), $W_h = 2.5$ mm, $T_h = 0.03$ mm, $L_h = 30$ mm, and $\theta_h = 2.7$ rad. The magnitude of the torque indicates that it is important to consider the weight of the structural layers when designing a large structure.

Our self-folding method is simple, it can be performed at low cost, and it is easily accessible using a home oven. Furthermore, the folding order could potentially be controlled by incorporating more than one contraction material that responds to different temperatures.

2.2 Precise Angle Control by V-fold Spans (Pop-up)

The folding method for a precise folding angle of a flat sheet as introduced in Section 2.1 is difficult in that we have two-dimensional material properties that have to be manipulated at the level of three-dimensional systems.[1] We focus on kinematically encodable folding angles that enable the control of a specific folding angle of a surface, which is inspired by a technique used for pop-up books. Figure 3 shows two major types of pop-up techniques: (a) parallel fold and (b) V-fold [14] (often called angle fold). The pop-up motion can be characterized with two kinematically coupled angles: the input angle (θ_{in}) and the output angle (θ_{out}). While θ_{in} and θ_{out} are linearly related in the case of parallel fold, they are nonlinearly proportional in the case of V-fold.

The transition from Figure 4a to 4c shows an example of our approach. We aim at a mountain fold and a valley fold as described in Figure 4a, respectively spanning θ_{out1} and θ_{out2} ($\theta_{out} \in (0 : \pi)$). We segment the surfaces and deploy as a multi-pleat pattern (Figure 4b). When all creases are unfolded simultaneously ($\theta_{in} \to 0$), the attributed kinematics yield the sheet morphology shown in Figure 4b. Thus the geometries characterizing the surfaces in Figure 4a can be encoded in the parameters of creases in Figure 4c. The angles in Figure 4c, α_1 and α_2 ($\alpha \in (0 : 2\pi)$), designate the output angles θ_{out1} and θ_{out2} at respective θ_{in}. Moreover, the edge lengths L_{H*} ($* \in [1, 2, 3]$) in Figure 4a can be encoded as the respective edge lengths in Figure 4c, and the widths along the

1 One contrasting approach is the so-called *thick origami approach* [32].

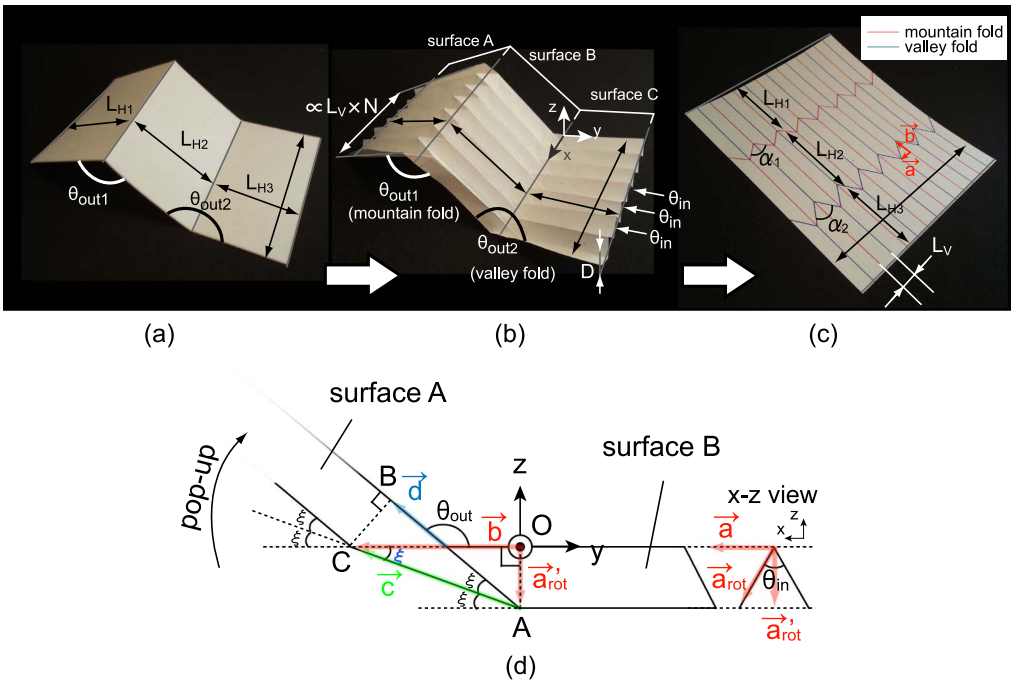

Figure 4. Encoding angled surface geometry in crease pattern. (a) Targeted angled surface. (b) Angle control by pleat accumulation. (c) Geometry of folding with respect to the input angle θ_{in} and the output angle θ_{out}. (d) Folding kinematics of V-fold.

x-axis in Figure 4a as the combination with L_V and the number of pleats, $N \in \mathbb{N}$. Namely, they are $\propto N \times L_V$. Finally, the thickness of the folded surfaces, D in Figure 4b, can be reduced by refining the resolution of pleats in accordance with $D \propto$ scale length. In summary, the methodology is to roughly control θ_{in} by the self-folding technique described in Section 2.1, and obtain θ_{out} in precision.

Figure 4d gives a side view of a valley V-fold, projected onto a y-z plane. We derive the relationship between θ_{in} and θ_{out} based on this schematic. We define constant vectors $\vec{a}$ and $\vec{b}$ shown in Figure 4c,d as

$$\vec{a} = [L_v \quad 0 \quad 0], \tag{2}$$

$$\vec{b} = \begin{bmatrix} 0 & -\dfrac{L_v}{\tan\dfrac{\alpha}{2}} & 0 \end{bmatrix}. \tag{3}$$

The rotation matrix about a unit vector $\vec{k} = [\kappa \quad \lambda \quad \mu]$ can be described using the rotation angle ϕ as

$$R(\kappa,\lambda,\mu,\phi) = \begin{bmatrix} \cos\phi + \kappa^2(1-\cos\phi) & \kappa\lambda(1-\cos\phi) - \mu\sin\phi & \kappa\mu(1-\cos\phi) + \lambda\sin\phi \\ \lambda\kappa(1-\cos\phi) + \mu\sin\phi & \cos\phi + \lambda^2(1-\cos\phi) & \lambda\mu(1-\cos\phi) - \kappa\sin\phi \\ \mu\kappa(1-\cos\phi) - \lambda\sin\phi & \mu\lambda(1-\cos\phi) + \kappa\sin\phi & \cos\phi + \mu^2(1-\cos\phi) \end{bmatrix}. \tag{4}$$

If the input angle is θ_{in} ($\theta_{in} : \pi \rightarrow 0$), then $\vec{a}_{\text{rot}}$, which is the tangent vector along the plane, is

$$\vec{a}_{\text{rot}} = \vec{a}\, R\left(0, -1, 0, \frac{\pi - \theta_{\text{in}}}{2}\right). \tag{5}$$

The projection of $\vec{a}_{\text{rot}}$ onto the y-z plane, $\vec{a}'_{\text{rot}}$, is

$$\vec{a}'_{\text{rot}} = \vec{a}_{\text{rot}} \begin{bmatrix} 0 & 0 & 0 \\ 0 & 1 & 0 \\ 0 & 0 & 1 \end{bmatrix}.$$

Since $\vec{c} = \vec{b} - \vec{a}'_{\text{rot}}$, and considering that $\triangle$OAC and $\triangle$BCA are homologous, $\vec{d}$ can be obtained by rotating $\vec{c}$ through the angle ξ, and adjusted to a desired length by scaling by a constant $s (s \in \mathbb{R})$, as

$$\vec{d} = s\ \vec{c}\ R(-1, 0, 0, \xi), \tag{6}$$

where $\xi = \arccos \frac{\vec{b} \cdot \vec{c}}{|\vec{b}||\vec{c}|}$. The targeted output angle θ_{out} can be derived by measuring the angle between $\vec{b}$ and $\vec{d}$ as

$$\theta_{\text{out}} = \arccos \frac{-\vec{b} \cdot \vec{d}}{|-\vec{b}||\vec{d}|}. \tag{7}$$

We define the *completion* of a V-fold as

$$\text{completion } [\%] = \frac{\pi - \theta_{\text{out}}}{\pi - \theta_{\text{out}}|_{\theta_{\text{in}} = 0}} \times 100, \tag{8}$$

as an indication of the accomplishment degree of a targeted folding (pop-up) angle.

Figure 5a shows the relation between θ_{in} and completion with different α varying from $\alpha = 30°$ to $\alpha = 150°$ in five levels. It can be seen that the convergence of completion has good speeds: 80% of the folding angles are already accomplished at $\theta_{\text{in}} \approx 90°$, especially when $\alpha > 90°$. Since actual convergence of θ_{out} when self-folding is determined by the physical factors (e.g., applied temperature, internal stress of PVC, and gap widths of hinges), it settles at $\theta_{\text{in}} < 90°$ (finely tunable). Figure 5a shows that the larger α becomes, the faster the folding is. By considering these physical tendencies, the actual folding angles can be preadjusted by setting wider α to obtain precise folding angles θ_{out}.

Figure 5b shows the angle θ_{in} required to gain a desired completion for different α. Attaining smaller θ_{in} requires more compression of the contraction layer and thus requires more heat input. The data shows that the larger α is, the less energy is required. Also, 70% completion can be attained for most α even if θ_{in} does not become less than 90°.

2.3 Fabrication of Self-folding Crease Pattern

Manually folding a multi-crease structure is a time-consuming process. When the folding steps are on the order of dozens, or multiple creases need to be folded simultaneously, self-folding can greatly reduce the total fabrication time. In this subsection, we introduce a fabrication method for self-folding that is simple and fast, but also accurate and easily reproducible. The key insight is that the folding directions are determined by the gap width differences of the hinge parts (Section 2.1). The methodology is to sustain both the front and the back side of the structural materials' relative positions on a single supporting sheet, and sandwich a contraction layer by folding it in half, so that corresponding gaps come above and below the contraction layer (Figure 6).

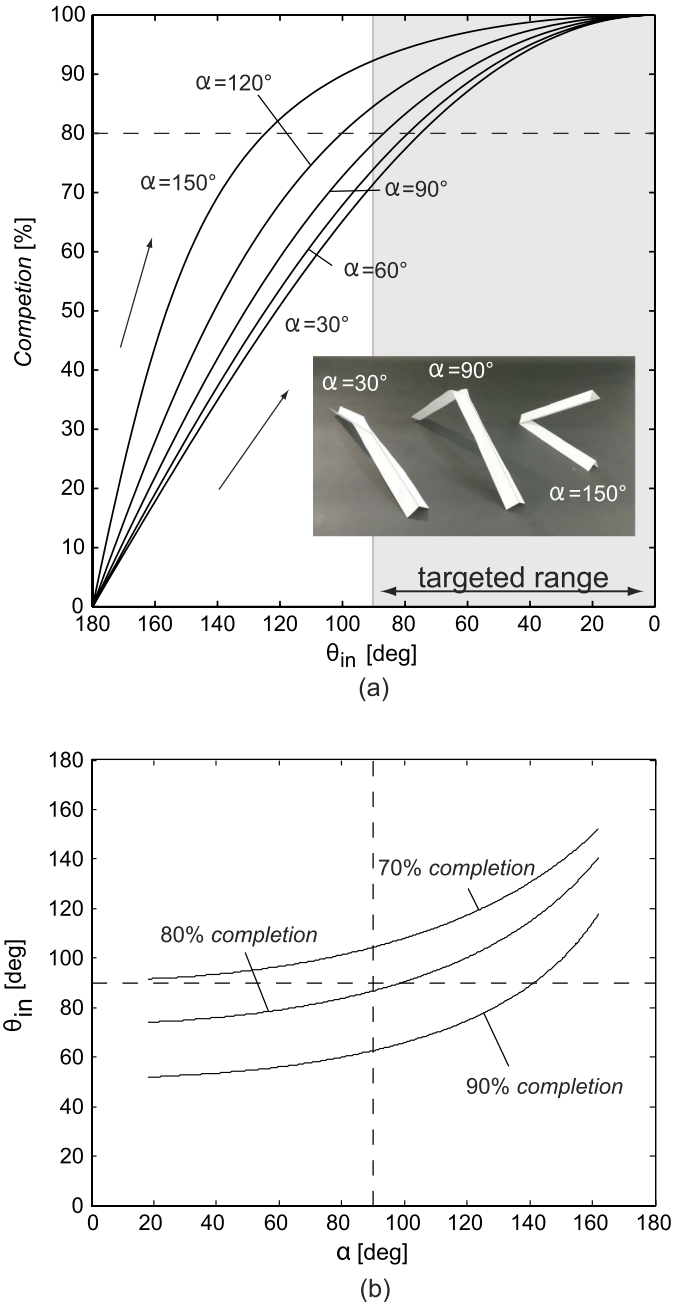

Figure 5. (a) Convergence of θ_{out} in correspondence with θ_{in} with different α. (b) θ_{in} required to gain a desired completion for different α.

First, the supporting layer (Post-it Sheet Labels and 3M Permanent Adhesive Full Sheet Labels) and the structural layer (Grafix Ink Jet Adhesive Film, thickness 0.12 mm) are laminated, so that the adhesive face of the structural layer faces out (Figure 6a). Using a laser cutting machine (Versa-LASER, VLS 3.50) with regulated laser strength, we cut only through the structural layer and trim the front and back patterns (Figure 6b). The framelike segments of structural layers that cover the

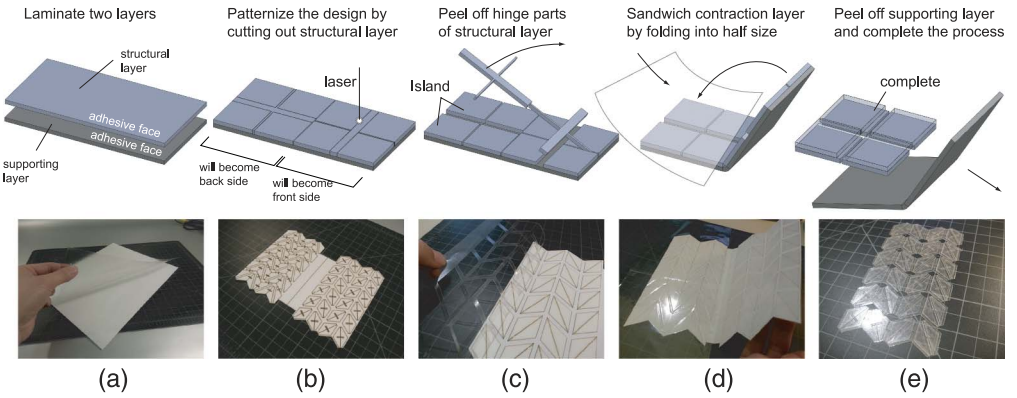

Figure 6. Fabrication process of self-folding multi-crease pattern. Structural materials are placed in designed gap widths on the front and back of the contraction layer.

hinge parts are peeled off (Figure 6c). A contraction layer (PVC, thickness 0.03 mm) is inserted and sandwiched by folding the structural layer in half, so that the respective hinges overlap above and below the contraction layer (Figure 6d). We manually cut out the intersections of hinges using a cutter, where six creases are gathered. This process was incorporated on account of some bending direction errors we often encountered when heating up. However, further investigation is still required to conclude if this step is necessary. We peel off the supporting layer, and obtain the complete structure (Figure 6e). The complete structure has thickness 0.27 mm and size 70 × 125 mm^2. This fabrication method has an advantage with forms where large-scale shapes are formed by iterative crease accumulations.

3 Self-folding and Proof of Concept in Robotics

In this section, we show how our self-folding method can be used to make a mobile robot. We show that a self-folded skeleton can function as a stabilizer of locomotion and perform basic locomotion when coupled with an easily implementable actuation unit (Figure 1).

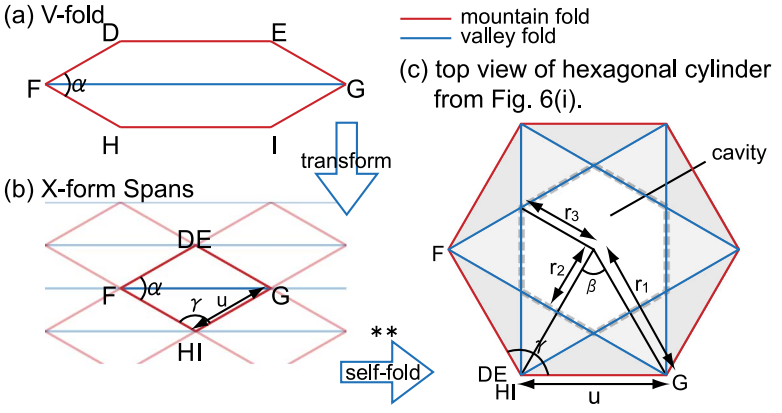

Figure 7. X-form spans, which are an extension of the V-fold: (a) V-fold, (b) X-form spans, and (c) side view after completed folds. ** Alternate the direction of every second row.

3.1 Structure Design for a Self-folded Cylindrical Robot

The outer skeleton of the robot is a hollow cylindrical structure with symmetry, simplicity, and postural robustness. The pleat pattern, the X-form span, is one of the most complex foldings among V-folds, where intersections gather six creases, thus posing a significant self-folding challenge.

Figure 7a shows two V-folds (colored red), whose spanning angles are α, interleaving a valley fold (colored blue). For the formation of the 3D structure, we aim at a cylindrical shape using X-form spans, which can be regarded as an extension of the V-fold (Figure 7b). The X-form spans can be derived by transforming the V-fold; from Figure 7a, we shorten the distances D-E and H-I, and configure a rhombus. When arrays of this rhombus are folded, a regular n-sided polygonal cylinder is generated (the hexagonal case is shown in Figure 7c in top view). Two design parameters, α and u, can be determined by examining the geometry of the hollow cavity that will be created in the folded n-sided polygonal structure. When the geometric parameters of the actuation unit (r_2, r_3, and n) are given, these designing parameters are determined as

$$\alpha = \frac{\pi}{2} - \frac{n-2}{n}\pi, \tag{9}$$

$$u = \frac{2\sin\frac{\pi}{n}}{\cos\frac{2\pi}{n}} \times r_2 \tag{10}$$

$$= \tan\frac{2\pi}{n} \times r_3. \tag{11}$$

Instead of rhombus X-form spans, more general models of origami-inspired polygonal cylinders have been investigated in [10, 20]. The size of the body and the resolution of the pleats can vary. We selected a hexagonal shape because the resulting folded outer skeleton has sufficient volume to include all the robot's components, and at the same time the flat patches provide support and friction for locomotion. Our designed robot will use the flat areas to contact the ground and control slippage. The arrays of rhombuses are alternately redirected, so that when the sheet folds, zigzag-shaped edges naturally latch and thus the structure is stable (see Figure 2g). We set $\alpha = 60°$, $u = 20$ mm, gap width = 2.5 mm, bridge width = 1 mm. The designed shape consists of 62 creases that must be folded simultaneously; thus, they are difficult to fold by hand.

3.2 Self-folding Process

Figure 8 shows the self-folding process performed in a heat oven. In order to transmit uniform heat to the sheet, the sheet was hung from the ceiling. This setting contributes to preventing direct physical

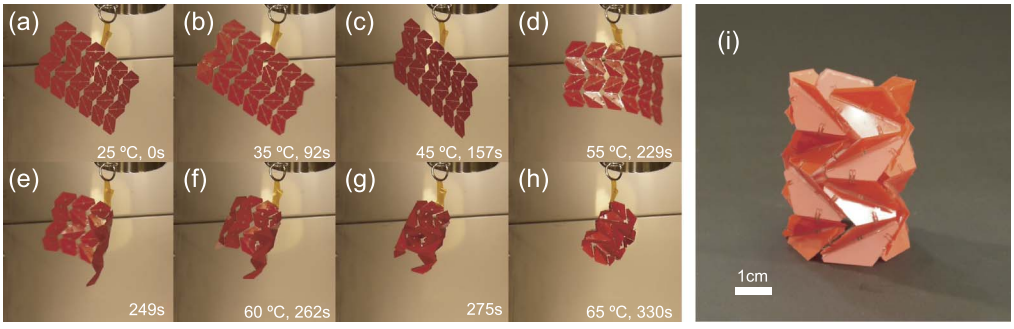

Figure 8. Self-folding attained by baking in a heat oven.

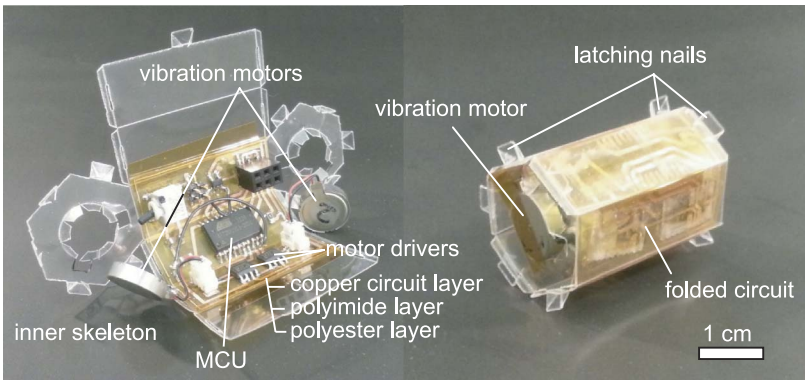

Figure 9. Encapsulated actuation unit. (a) Self-folded inner skeleton and flexible circuit with components. (b) Flexible circuit folded into hexagonal cylindrical shape.

contact with the heat source (generally the bottom of the oven). The oven we employed blows air from the side wall, and thus the sheet swings during the process.[2]

We ramped the temperature from room temperature (25°C) to 65°C (Figure 8a). When the temperature reached approximately 55°C, the crease pattern appeared on the sheet's surface, increasing the sculpture effect and forming a global curve (Figure 8d–g). When the temperature reached 65°C, the structure formed a complete cylindrical shape, automatically latching both sides via zigzag tooth-shaped edges (Figure 8h). The process was completed in approximately 5 min. The duration depends on the capability of the oven, as well as the size of the materials, and should be optimized according to conditions.

Note that the configured shape is made of 62 folds; that is, the failure rate of an individual build up fold must be at most $\frac{1}{62} \times 100 = 1.61\%$. We have made four trials and encountered no error. As found in previous failure models, it is required that all 62 folds be completed without a failure. Should even one fold fail, the global structure becomes a distorted flat sheet.

3.3 Mechatronics

A modularized actuation unit, which shapes the hexagonal cylinder to fit to the outer skeleton, is developed. The actuation unit features collaterally assigned vibration motors for locomotion. By alternating the movement of vibration motors, the robot can move to any planar configuration, according to [11, 21, 30] (Figure 9b). The controller board was developed on a printed flexible circuit, whose folded geometry fits into the actuation unit. Finally, the actuation unit is manually inserted and attached to the outer skeleton. The projecting nails cause the actuation unit to reside stably in the outer skeleton.

The circuit is printed onto a sheet layer and then folded. The circuit substrate is composed of three sheet materials: one with rigid stiffness, used as a backbone layer (polystyrene); another with heat-resistive properties (polyimide); and the third conductive (copper). After these layers are laminated into one sheet, coating material is sputtered onto the copper layer in the shape of a circuit using a solid-ink printer. The remaining intact copper material is then etched by being soaked in ferric chloride for about 15 min, and is scrubbed away. Slits are added using a cutter, and bent manually to fit into the inner skeleton that was previously cut by a laser cutting machine and folded. The fabricated layer is resistant to heat, but is also lightweight at 0.442 g. We list the components used in the robot in Table 1.

2 The air blow is an intrinsic functionality of the oven that we could not stop; however, we assume the influence of the blow is not essential, judging from smaller-scale trials in an ordinary oven.

Table 1. Components used in the robot.

Device	Weight [g]	Type
Outer skeleton	1.966	Self-folded
MCU	0.561	ATtiny2313A, Atmel
Vibration motor	1.390 × 2	1.8 G, T.P.C.
Flexible circuit layer	0.442	Printed on 3 layers
Other SMD components	0.283	Switch, etc.
Connectors	1.526	ISP Connectors, etc.
LiPo battery	1.773	40 mA h, Great Power battery
Inner skeleton and others	1.428	Cage, cables, solder
Total weight	10.759	

The controller consists of a micro control unit (MCU), two vibration motors with respective motor drivers, electricity-regulating components, a battery, and other accessories, such as connectors. We selected the Atmel ATtiny2313A for its low operation voltage and for its serial communication capability for future use. Since the circuit becomes part of the robot, the weight distribution of components was considered and designed.

Figure 10 shows the weight distribution plotted in a pie chart. The body (outer skeleton) contributes only 18.27% of the weight, which is remarkably little, and shows the merits of forming a body through foldings.

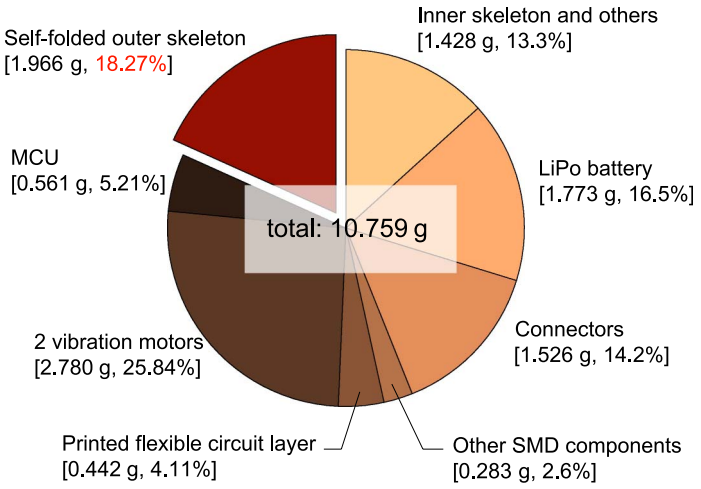

Figure 10. Weight distribution of the robot.

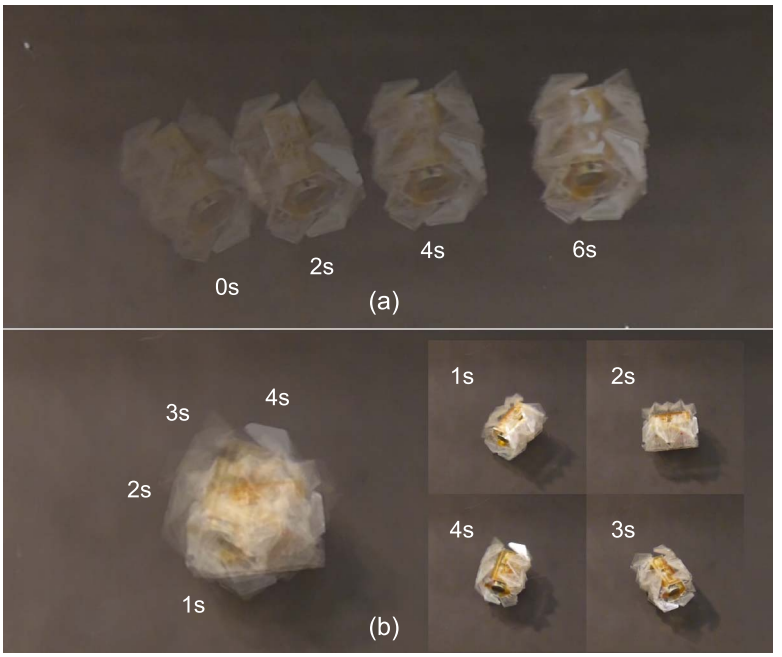

Figure 11. Results of motions. (a) Translational motion by turning the two motors in the same direction. (b) Rotational motion by turning in opposite directions.

3.4 Results

Figure 11 shows the demonstrated locomotions. Control of the actuators is managed by an open-loop control, whose driving current is managed by pulse width modulation (duty ratio = 50%). It is seen that both translational (Figure 11a) and rotational (Figure 11b) motions are achieved by altering the directions of rotation of the vibration motors. When moving forward, we turn both motors in the same direction, and the translational locomotion speed is 2.95 cm/s. When turning, the motors turn in opposite directions, and the robot's turning angular speed is 0.74 rad/s (42.4°/s). However, especially for the translational motion, the motion is sensitive to the friction of the ground, and does not necessarily happen at the same speed on changing the motor speeds. We also assume that the asymmetric pleat patterns will have an influence on the stability of motion.

4 Conclusion

This article presents a scheme for self-folding for the autonomous fabrication of an origami robot using global heating. We first develop a method that enables autonomous and simultaneous folds of mountain and valley creases in a sheet structure. We then focus on the characteristics of the V-fold spans, where one of the angles can be precisely controlled by kinematically coupling it to another angle. The X-form span mechanism is then incorporated as an extension of V-fold. Using uniform heat on the designed sheet in this fashion, a cylindrical robot body is attained. We developed an easy, fast, and reliable fabrication technique for constructing the self-folding sheet. The self-folding process completes in approximately 5 min, where 62 folds are simultaneously managed at 65°C. We further develop a mobile robot using this self-folded body. The robot has two vibration motors for locomotion, caged by the self-folded outer skeleton for stabilization. The robot's locomotion proves the functionality of a self-folded origami structure.

Acknowledgment

This research was conducted in the Distributed Robotics Laboratory at CSAIL, MIT. Support for this work has been partly provided by NSF grants 1240383 and 1138967, and the Swiss National Science Foundation Fellowship Grant PA00P2_142208.

References

1. Brodbeck, L., & Iida, F. (2012). Enhanced robotic body extension with modular units. In *IEEE/RSJ International Conference on Intelligent Robots and Systems (IROS)* (pp. 1428–1433).
2. Cheung, K. C., Demaine, E. D., Bachrach, J. R., & Griffith, S. (2011). Programmable assembly with universally foldable strings (moteins). *IEEE Transactions on Robotics*, *27*, 718–729.
3. Felton, S. M., Tolley, M. T., Onal, C. D., Rus, D., & Wood, R. J. (2013). Robot self-assembly by folding: A printed inchworm robot. In *IEEE International Conference on Robotics and Automation (ICRA)* (pp. 277–282).
4. Fukuda, T., & Kawauch, Y. (1990). Cellular robotic system (CEBOT) as one of the realizations of self-organizing intelligent universal manipulator. In *IEEE International Conference on Robotics and Automation (ICRA)* (pp. 662–667).
5. Griffith, S., Goldwater, D., & Jacobson, J. (2005). Self-replication from random parts. *Nature*, *437*, 636.
6. Guan, J., He, H., Hansford, D. J., & Lee, L. J. (2005). Self-folding of three-dimensional hydrogel microstructures. *The Journal of Physical Chemistry B*, *109*, 23134–23137.
7. Hawkes, E., An, B., Benbernou, N. M., Tanaka, H., Kim, S., Demaine, E. D., Rus, D., & Wood, R. J. (2010). Programmable matter by folding. *Proceedings of the National Academy of Sciences of the U.S.A.*, *107*(28), 12441–12445.
8. Hoffman, K. L., & Wood, R. J. (2010). Towards a multi-segment ambulatory microrobot. In *IEEE International Conference on Robotics and Automation (ICRA)* (pp. 1196–1202).
9. Hoover, A. M., Steltz, E., & Fearing, R. S. (2008). RoACH: An autonomous 2.4 g crawling hexapod robot. In *IEEE/RSJ International Conference on Intelligent Robots and Systems (IROS)* (pp. 26–33).
10. Hunt, G. W., & Ario, I. (2005). Twist buckling and the foldable cylinder: An exercise in origami. *International Journal of Non-linear Mechanics*, *40*, 833–843.
11. Ioi, K. (1999). A mobile micro-robot using centrifugal forces. In *IEEE/ASME International Conference on Advanced Intelligence Mechatronics* (pp. 736–741).
12. Ionov, L. (2011). Soft microorigami: Self-folding polymer films. *Soft Matter*, *7*, 6786–6791.
13. Iwase, E., & Shimoyama, I. (2005). Multistep sequential batch assembly of three-dimensional ferromagnetic microstructures with elastic hinges. *Journal of Microelectromechanical Systems*, *14*, 1265–1271.
14. Jackson, P. (2011). *Folding Techniques for Designers from Sheet to Form*. London: Laurence King.
15. Klavins, E. (2007). Programmable self-assembly. *IEEE Control System Magazine*, *27*, 43–56.
16. Kotay, K., Rus, D., Vona, M., & McGray, C. (1998). The self-reconfiguring robotic molecule. In *IEEE/RSJ International Conference on Intelligent Robots and Systems (IROS)* (pp. 424–431).
17. Liu, Y., Boyles, J. K., Genzer, J., & Dickey, M. D. (2011). Self-folding of polymer sheets using local light absorption. *Soft Matter*, *8*, 1764–1769.
18. Martinez, R. V., Fish, C. R., Chen, X., & Whitesides, G. M. (2012). Elastomeric origami: Programmable paper-elastomer composites as pneumatic actuators. *Advanced Functional Materials*, *22*, 13761384.
19. Mermoud, G., Mastrangeli, M., Upadhyay, U., & Martinoli, A. (2012). Real-time automated modeling and control of self-assembling systems. In *IEEE International Conference on Robotics and Automation (ICRA)* (pp. 4266–4273).
20. Min, C. C., & Suzuki, H. (2008). Geometrical properties of paper spring. In *Manufacturing Systems and Technologies for the New Frontier* (pp. 159–162).
21. Miyashita, S., Casanova, F., Lungarella, M., & Rolf Pfeifer, F. (2008). Peltier-based freeze-thaw connector for waterborne self-assembly systems. In *IEEE/RSJ International Conference on Intelligent Robots and Systems (IROS)* (pp. 1325–1330).

22. Miyashita, S., Göldi, M., & Pfeifer, R. (2001). How reverse reactions influence the yield rate of stochastic self-assembly. *International Journal of Robotics Research*, *30*(April), 627–641.

23. Miyashita, S., Onal, C. D., & Rus, D. (2013). Self-pop-up cylindrical structure by global heating. In *IEEE/RSJ International Conference on Intelligent Robots and Systems (IROS)*.

24. Miyashita, S., & Rus, D. (2013). Multi-crease self-folding by uniform heating. In *12th European Conference on Artificial Life (ECAL)*.

25. Murata, S., Tomita, K., Yoshida, E., Kurokawa, H., & Kokaji, S. (1999). Self-reconfigurable robot. In *International Conference on Intelligent Autonomous Systems (IAS)* (pp. 911–917).

26. Nakano, K., Uchihashi, S., Umemoto, N., & Nakagama, H. (1994). An approach to evolutional system. In *First IEEE Conference on Evolutionary Computation (CEC)* (pp. 781–786).

27. Onal, C. D., Wood, R. J., & Rus, D. (2011). Towards printable robotics: Origami-inspired planar fabrication of three-dimensional mechanisms. In *IEEE International Conference on Robotics and Automation (ICRA)* (pp. 4608–4613).

28. Onal, C. D., Wood, R. J., & Rus, D. (2013). An origami-inspired approach to worm robots. *IEEE/ASME Transactions on Mechatronics*, *18*, 430–438.

29. Rothemund, P. W. K. (2006). Folding DNA to create nanoscale shapes and patterns. *Nature*, *440*(7082), 297–302.

30. Rubenstein, M., Ahler, C., & Nagpal, R. (2012). Kilobot: A low cost scalable robot system for collective behaviors. In *IEEE International Conference on Robotics and Automation (ICRA)* (pp. 3293–3298).

31. Ryu, J., D'Amato, M., Cui, X., Long, K. N., Qi, H. J., & Dunn, M. L. (2012). Photo-origamibending and folding polymers with light. *Applied Physics Letters*, *100*, 161908-1–5.

32. Tachi, T. (2011). Rigid-foldable thick origami. In Patsy Wang-Iverson, Robert J. Lang, & Mark Yim (Eds.), *Origami 5: Fifth International Meeting of Origami in Science, Mathematics, and Education*, (pp. 253–264), Boca Roton, FL: CRC Press.

33. Tolley, M., Felton, S., Miyashita, S., Xu, L., Shin, B., Zhou, M., Rus, D., & Wood, R. (2013). Self-folding shape memory laminates for automated fabrication. In *IEEE/RSJ International Conference on Intelligent Robots and Systems (IROS)*.

34. Whitney, J., Sreetharan, P., Ma, K., & Wood, R. (2011). Pop-up book MEMS. *Journal of Micromechanics and Microengineering*, *21*(11), 115021.

35. Yim, M. (1994). New locomotion gaits. In *IEEE International Conference on Robotics and Automation (ICRA)* (pp. 2508–2514).